



LAWRENCE
LIVERMORE
NATIONAL
LABORATORY

Multi-Period Restoration Model for Integrated Power-Hydrogen Systems Considering Transportation States

Z. Wang, T. Ding, W. Jia, C. Mu, C. Huang, J.
Catalao

October 13, 2021

IEEE Transactions on Industry Applications

Disclaimer

This document was prepared as an account of work sponsored by an agency of the United States government. Neither the United States government nor Lawrence Livermore National Security, LLC, nor any of their employees makes any warranty, expressed or implied, or assumes any legal liability or responsibility for the accuracy, completeness, or usefulness of any information, apparatus, product, or process disclosed, or represents that its use would not infringe privately owned rights. Reference herein to any specific commercial product, process, or service by trade name, trademark, manufacturer, or otherwise does not necessarily constitute or imply its endorsement, recommendation, or favoring by the United States government or Lawrence Livermore National Security, LLC. The views and opinions of authors expressed herein do not necessarily state or reflect those of the United States government or Lawrence Livermore National Security, LLC, and shall not be used for advertising or product endorsement purposes.

Multi-Period Restoration Model for Integrated Power-Hydrogen Systems Considering Transportation States

Zekai Wang, *Student Member, IEEE*, Tao Ding, *Senior Member, IEEE*, Wenhao Jia, *Student Member, IEEE*, Can Huang, *Senior Member, IEEE*, João P. S. Catalão, *Senior Member, IEEE*,

Abstract—This paper proposes an integrated power and hydrogen distribution system (IPHDS) restoration model in response to multiple outages caused by natural disasters. During the restoration, repair crews (RCs) and mobile battery-carried vehicles (MBCVs) are considered to repair faulted lines and support critical power loads. Also, the network reconfiguration is taken into consideration in the restoration model to pick up loads. Besides, to address the different response time of hydrogen and power systems, the aerodynamic law-based dynamic hydrogen flow model is applied in the hydrogen system. The proposed model is presented as a mixed-integer linear program which is verified on a 33-bus-48-node IPHDS with multiple outages. The present results verify the effectiveness of the proposed method.

Index Terms—Resilience, integrated power and hydrogen distribution system restoration, repair crews, mobile battery-carried vehicles, dynamic hydrogen flow, network reconfiguration.

I. INTRODUCTION

DU^E to the global climate change, extreme weather events, e.g., hurricanes, windstorms, and typhoons, have become increasingly frequent and devastating in recent years, causing increasing power outages and infrastructure damages [1]-[3]. For instance, Hurricane Sandy in 2012 brought severe damages to the power distribution systems, which led to 8.66 million customer outages [4]. Furthermore, more than 80% of power outages in the U.S. were attributed to natural disasters, and approximately 90% of them were caused by failures in distribution systems [5], [6]. Hence, it is of critical importance to enhance the resilience of power distribution systems against extreme natural disasters [7]-[17].

In [7], a robust optimization-based approach was proposed for the optimal planning of resilient distribution networks, which considered the distributed generation resource placement and grid hardening strategies. Reference [8] proposed a two-stage robust optimization framework for the optimal line hardening of the resilient distribution systems with multiple renewable resources. Based on deep reinforcement learning, a long-term planning model based on hardening strategies was proposed in [9] to improve the resilience of power distribution systems. In [10], a sequential service restoration model was

formulated for distribution systems and microgrids in extreme power outage events by coordinating the distributed generators and switches. Also, [11] developed a risk-limiting load restoration approach to enhance the resilience of distribution systems with networked microgrids.

In addition, network reconfiguration is also an efficient method for the resilience enhancement of distribution systems [12]-[16]. Reference [17] proposed an optimal load restoration model for enhancing the distribution system resilience by utilizing the network reconfiguration and microgrid formation. Based on the topology reconfiguration and distributed generator islanding, a tri-level defender-attacker-defender framework for the resilient distribution systems was formulated in [13]. A unified two-stage reconfiguration model was established in [14] to improve the resilience of distribution networks, and the scenario decomposition method was employed to relieve the computation burden. In [15], a resilience enhancement strategy for distribution systems was presented considering islanding and dynamic reconfiguration. In [16], a novel formulation was proposed for radiality constraints to increase the flexibilities in the network reconfiguration-related optimization problems of distribution systems. Considering the network reconfiguration and distributed generators scheduling, [17] proposed a power outage management strategy for the enhancing the resilience of distribution network.

The above papers were mainly focused on the resilience of power distribution systems, while neglecting the impact of other energy systems such as natural gas and hydrogen. In recent years, with the continuous progress in power-to-gas (P2G) technology, the electric hydrogen production (EHP) becomes feasible and economical, which can provide enormous flexibilities for power grids to accommodate the intermittent power supply from renewable energy resources [18]. Therefore, the integrated power-hydrogen system (IPHS) will play a crucial role in the future energy transformation and low-carbon pathways. Several papers have studied the optimal planning and operation of the IPHS [19]-[24]. Reference [19] proposed a robust IPHS planning model which considered the power to hydrogen and heat, seasonal hydrogen storage, and N-1 reliability constraints of crucial devices. Reference [20] formulated an optimal operation framework for the IPHS with utilization of hydrogen fuel cell vehicles. In [21], a hybrid IPHS energy sharing framework was presented considering the P2G devices and plug-in hybrid electric-hydrogen vehicles. In [22], an optimal dispatch model was established for the active distribution systems considering the power-to-hydrogen-and-heat scheme. Additionally, reference [23] proposed a security constrained unit commitment model with integration of P2G devices and hydrogen gas

Z. Wang, T. Ding and W. Jia are with the Department of Electrical Engineering, Xi'an Jiaotong University, Xi'an, Shaanxi, 710049, China. (email: tding15@mail.xjtu.edu.cn)

C. Huang is with Lawrence Livermore National Laboratory, Livermore, CA 94550, USA.

J. P. S. Catalão is with the Faculty of Engineering of the University of Porto (FEUP) and INESC TEC, Porto, Portugal.

This work was performed under the auspices of the U.S. Department of Energy by Lawrence Livermore National Laboratory under Contract DE-AC52-07NA27344 with Release Number LLNL-JRNL-827835.

turbines. Reference [24] proposed a joint optimization model for the power-hydrogen-heat energy systems to reduce the wind and solar power curtailment.

Furthermore, the increasing interdependency between power distribution systems and hydrogen systems will also bring extraordinary challenges to the resilience of the IPHS. In addition to the electric infrastructures, the key components of hydrogen systems, such as EHPs, pipelines, storage tanks, compressors, and gas-fired units, may also get damaged by natural disasters, which makes the IPHS disaster restoration more complicated. Therefore, the existing methodologies for the power distribution system resilience [7]-[17] may no longer apply to the resilience of the IPHS. It is necessary to mathematically characterize the new features of the IPHS, such as the transient modeling of hydrogen pipeline flow and EHP process, to set up a hybrid disaster restoration framework for the IPHS. However, all these issues have not yet been sufficiently discussed in the current publications.

Emergency response resources, such as the repair crews (RCs) and mobile power sources (MPSs), can be dispatched to the desired fields through the transportation network, providing flexibilities for the restoration strategies of the IPHS [25]-[27]. In essence, the optimal dispatch of RRCs and MPSs can be equivalent to a classical vehicle routing problem [28], [29]. Considering the hybrid dispatch of RRCs and MPSs in the transportation network, reference [30] proposed an optimal load restoration approach for the resilient distribution systems. In [31], a two-stage outage management strategy was suggested by co-optimizing the RRCs, topology reconfiguration, and distributed generation dispatch. Reference [32] proposed a three-stage stochastic optimization model by fully incorporating the optimal planning, pre-position, and dispatch of MPSs, thus minimizing the investment costs and improving the system resilience. In [33], a multiperiod restoration framework was proposed for the resilient distribution systems by optimally coordinating the RCs, mobile battery-carried vehicles (MBCVs), and networked microgrids formation.

In this paper, we proposed a comprehensive multi-period restoration model (MPRM) for integrated power and hydrogen distribution system (IPHDS) under natural disasters with the coordination of RCs and MBCVs, and the dynamic delivery process of hydrogen is also taken into consideration. The main contributions can be summarized as follows:

(i) We proposed an IPHDS model, in which the power system and the hydrogen system are connected by electric hydrogen production devices (EHPs) and hydrogen-fired units. During load restoration, the aerodynamic laws for the hydrogen delivery in pipelines are considered in the hydrogen model.

(ii) A multi-period co-optimization model is set up for RCs and MBCVs, producing a mixed-integer linear program model. Since the transportation state keeps changing during the restoration process, the ever-changing travel times for RCs and MBCVs are also taken into consideration in the proposed model.

The rest of the paper is summarized as follows. Section II details the modeling of three technologies: RCs, MBCVs, and dynamic hydrogen flow. Section III sets up the optimization MPRM model for the IPHDS with three technologies. Section IV studies and analyzes two cases for distribution network restoration. Section V concludes this paper.

II. MATHEMATICAL MODELING OF RCs, MBCVs AND DYNAMIC HYDROGEN FLOW

In this part, the models of RCs, MBCVs, and dynamic hydrogen flow are respectively set up for IPHDS restoration. Note that RCs and MBCVs have their own routes and are easily influenced by transportation state. The transportation state and travel time variability are considered in the model of RCs and MBCVs. Besides, since the hydrogen flow constraints are non-linear functions, a linearization method is used for the dynamic hydrogen flow to facilitate the computational burden.

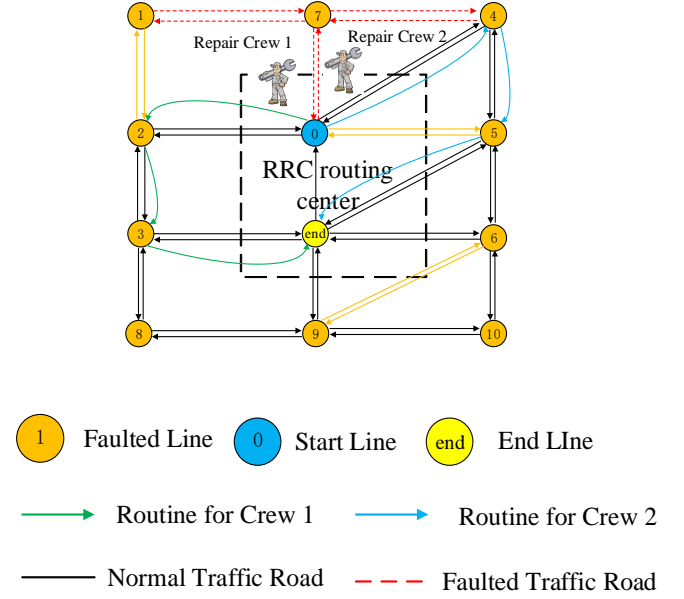


Fig. 1. An example of RRCs

A. Modeling of Repair Crews

RCs are a kind of important resilient resources in IPHDS restoration. In a restoration process, RCs can be modeled as a routing problem which can be formulated by the graph theory [34]. To explain the model of RCs, we assume that N lines are damaged in a natural disaster. Then we can define a graph $H_K = (\Psi^{KA}, \Psi^{KL})$, and $\{0, 1, 2, 3, \dots, N, end\}$ is the index for the set of faulted lines, where "0" and "end" both represent the RC route center. In a RC route, the repair crew should leave from the faulted line "0" to repair lines and return to faulted line "end" after repairing tasks. Fig. 1 shows an example of two RCs, including the travel routes of RC1 and RC2 which are $Route_1 = \{0, 2, 3, end\}$ and $Route_2 = \{0, 4, 5, end\}$. To guarantee that all RC routes start from "0" and return to "end" after repairing tasks are finished, we should have

$$\sum_{n \in \Psi^{KA}} M_{0,n,c}^{crew} - \sum_{m \in \Psi^{KA}} M_{m,0,c}^{crew} = 1, \forall c \quad (1)$$

$$\sum_{m \in \Psi^{KA}} M_{m,end,c}^{crew} - \sum_{n \in \Psi^{KA}} M_{end,n,c}^{crew} = 1, \forall c \quad (2)$$

where $M_{0,n,c}^{crew}$ is a binary variable that shows whether crew c travels from line 0 to line n . $M_{m,0,c}^{crew}$ is a binary variable that shows whether crew c travels from line m to line 0. $M_{m,end,c}^{crew}$ is a binary variable that shows whether crew c travels from line m to line end. $M_{end,n,c}^{crew}$ is a binary variable that shows whether crew c travels from line end to line n . For example, for RC1 in $Route_1$, we have $M_{0,2,1}^{crew} = M_{2,3,1}^{crew} = M_{3,end,1}^{crew} = 1$, and others are 0. Ψ^{KA} denotes the set of the faulted lines. It worth noting that Ψ^{KA} contains not only faulted power lines but also faulted hydrogen pipelines.

Moreover, the repair process should be continuous and each component should be repaired only once. Therefore, we have

$$R_{i,c} = \sum_{m \in \Psi^{KA}} M_{m,i,c}^{crew}, \forall i \in \Psi^{KA} \quad (3)$$

$$\sum_{\forall c} R_{i,c} = 1, \forall i \in \Psi^{KA} \quad (4)$$

where $R_{i,c}$ is a binary variable that indicates whether faulted line i is repaired by RC c . $M_{m,i,c}^{crew}$ is a binary variable that indicates whether RC c travels from m to i during the restoration.

Since each RC which leaves to repair a faulted line must return to the crew center after all repairing tasks, the number of RCs which leave each line should be equal to the number of RCs that arrive at this line. Thus, we have

$$\sum_{n \in \Psi^{KA}} M_{s,n,c}^{crew} - \sum_{m \in \Psi^{KA}} M_{m,s,c}^{crew} = 0, \forall s \in \Psi^{KA}, \forall c \quad (5)$$

where $M_{s,n,c}^{crew}$ is a binary variable that indicates whether RC c travels from s to n during the restoration. $M_{m,s,c}^{crew}$ is a binary variable that indicates whether RC c travels from m to s during the restoration.

Besides, the repair and travel time for each RC should also be formulated. To explain the time constraints for each RC, we still take Fig. 1 as an example. RC1 arrives at line 2 at $T_{2,1}^{crew} = T_{0,1}^{crew} + t_{0,2,l}$, $l = T_{0,1}^{crew}$, and arrives at faulted line 3 at $T_{3,1}^{crew} = T_{2,1}^{crew} + t_{2,3,l}$, $l = T_{2,1}^{crew} + t_{2,3,l}$. So, we can summarize that the faulted line m would be repaired and reconnected by the c -th RC after $T_{m,c}^{crew} + t_{m,c}^{crew}$. Thus, we have:

$$T_{0,c}^{crew} = 0, \forall c \quad (6)$$

$$-(1 - M_{m,n,c}^{crew})M \leq T_{m,c}^{crew} + t_{m,c}^{crew} + t_{m,n,l} - T_{n,c}^{crew} \quad (7)$$

$$\leq (1 - M_{m,n,c}^{crew})M, \forall (m,n) \in \Psi^{KL}, \forall c, l = T_{m,c}^{crew} + t_{m,c}^{crew}$$

$$\sum_{\forall i} f_{i,t}^m = 1, \forall i \in \Psi^{KA} \quad (8)$$

$$\sum_{\forall t} (t \square f_{i,t}^m) \geq \sum_{\forall c} (T_{i,c}^{crew} + t_{i,c}^{crew} R_{i,c}), \forall i \in \Psi^{KA} \quad (9)$$

$$\sum_{\forall t} (t \square f_{i,t}^m) \leq \sum_{\forall c} (T_{i,c}^{crew} + t_{i,c}^{crew} R_{i,c}) + 1 - \varepsilon, \forall i \in \Psi^{KA} \quad (10)$$

$$0 \leq M_{i,c}^{crew} \leq R_{i,c}M, \forall i \in \Psi^{KA}, \forall c \quad (11)$$

$$y_{s,r,t} \leq \sum_{\tau=1}^{t-1} f_{i,\tau}^m, \forall i \in \Psi^{KA}, \forall c \quad (12)$$

where $T_{0,c}^{crew}$ denotes the time when crew c arrives at line 0. $T_{m,c}^{crew}$ denotes the time when crew c arrives at line m ; $t_{m,c}^{crew}$ denotes the time for crew c to repair the line m . $t_{m,n,l}$ denotes the travel time for crew c from m to n at time l . Since the transportation state would be different at each time, the travel time for each road would be various according to the traffic congestion. $f_{i,t}^m$ is a binary variable that indicates at time t whether station i is repaired. ε denotes the error factor. t denotes the current time. $y_{s,r,t}$ is a binary variable indicating whether line (s, r) is connected at time t ; 1 is "connected" and 0 otherwise. Ψ^{KL} denotes the set of the roads connected to faulted lines. Also, Ψ^{KL} contains the roads connected to both faulted power lines and pipelines. Constraints (6)-(12) are crew time limits. Constraint (6) ensures that all crews start from the depot (marked as 0) immediately after the outage ($t = 0$). Constraint (7) is a big-M constraint to define the arrival time for each point in the graph. In constraint (7), we assume that a RC arriving at a faulted line will complete the line repair before departure. When $M_{m,n,c}^{crew} = 1$, RC c travels from m to n . This work was performed under the auspices of the U.S. Department of Energy by Lawrence Livermore National Laboratory under Contract DE-AC52-07NA27344 with Release Number LLNL-JRNL-827835.

n , spends $t_{m,n,l}$, $l = T_{m,c}^{crew} + t_{m,c}^{crew}$ on travel, and completes the repair at $t_{i,c}^{crew}$. And when $M_{m,n,c}^{crew} \neq 1$, M is defined as a large number so that the variables are affected. Constraint (8) implies that each faulted line would be repaired only once; $f_{i,t}^m$ means that the faulted line i repair is completed and the line is ready to be energized at time t . Constraints (9) and (10) combine the binary variable $f_{i,t}^m$ with integer variable $T_{i,c}^{crew}$ to limit the repair time for each faulted line. Constraint (11) guarantees that only crew c , which was used to repair line i , has a positive value of $T_{i,c}^{crew}$, otherwise, the sum of $T_{i,c}^{crew}$ for each crew c will not represent the time the crew arrives at faulted line i . Constraint (12) ensures that the line can be energized in the distribution system after the repair, and (8) ensures that every faulted lines would be repaired.

B. Modeling of Mobile Battery-Carried Vehicles

When an outage happens, MBCVs will be dispatched from the vehicle center to the charging station to support critical loads, especially the loads located in an island. After the critical loads are restored, the MBCV should travel to another charging station to support other loads. Similar to the RCs, the model of MBCVs can also be formulated by graph theory. Also, we can define a graph $H_G = (\Psi^{GA}, \Psi^{GL})$ with N charging stations, and $\{0, 1, 2, 3, \dots, N, end\}$ is the index for the set of charging station nodes, where "0" and "end" both represent the vehicle center. In an MBCV route, the MBCV should leave from the vehicle charging station "0" to support critical loads and return to the charging station "end" after charging tasks. Also, to guarantee that all MBCVs start from "0" and return to "end" after charging tasks are finished, there should be

$$\sum_{n \in \Psi^{GA}} M_{0,n,d}^{vehicle} - \sum_{m \in \Psi^{GA}} M_{m,0,d}^{vehicle} = 1, \forall d \quad (13)$$

$$\sum_{m \in \Psi^{GA}} M_{m,end,d}^{vehicle} - \sum_{n \in \Psi^{GA}} M_{end,n,d}^{vehicle} = 1, \forall d \quad (14)$$

where $M_{0,n,d}^{vehicle}$ is a binary variable that shows whether MBCV d travels from station 0 to station n . $M_{m,0,d}^{vehicle}$ is a binary variable that shows whether MBCV d travels from station m to station 0. $M_{m,end,d}^{vehicle}$ is a binary variable that shows whether MBCV d travels from station m to station end. $M_{end,n,d}^{vehicle}$ is a binary variable that shows whether MBCV d travels from station end to station n . Ψ^{GA} denotes the set of stations with plugs to MBCV.

Similarly, MBCVs that come to a charging station must leave when charging is completed, which leads to

$$\sum_{n \in \Psi^{GA}} M_{s,n,d}^{vehicle} - \sum_{m \in \Psi^{GA}} M_{m,s,d}^{vehicle} = 0, \forall s \in \Psi^{GA}, \forall d \quad (15)$$

Though there are many similar parts in the RC and MBCV models, there still exist three differences. Note that MBCVs can only support power load at charging station and cannot repair the faulted stations and lines. Therefore, functions (3) and (4) are not applied in the MBCV model. On the other hand, in the RC model, only one RC can repair a faulted line simultaneously. But in the model for MBCVs, it is normal that several MBCVs arrive at the same charging station, which means function (8) is not necessary in the MBCV model. Besides, the charging time of MBCVs at each station can be varied according to the demand, while the repair time for RCs at each faulted line is fixed. Thus, the charging and travel time constraints for MBCVs should be expressed as

$$T_{n,d}^{vehicle} = T_{m,d}^{vehicle} + t_{m,n,d,l}^{MBCV} + t_{m,d}^{vehicle}, \forall d, l = T_{m,d}^{vehicle} + t_{m,d}^{vehicle} \quad (16)$$

where $T_{n,d}^{vehicle}$ denotes the time when vehicle d arrives at the station n . $T_{m,d}^{vehicle}$ denotes the time when vehicle d arrives at station m . $t_{m,n,d,l}^{MBCV}$ denotes the travel time of MBCV d from m to n at time l . $t_{m,d}^{vehicle}$ denotes the time when vehicle d stays at station m . To characterize the relationship between $T_{m,c}^{vehicle}$ and $t_{m,n}^{MBCV}$, a big-M approach is employed by [35], where

$$-(1 - M_{m,n,d}^{vehicle})M \leq T_{m,d}^{vehicle} + t_{m,d}^{vehicle} + t_{m,n,d,l}^{MBCV} - T_{n,d}^{vehicle} \quad (17)$$

$$\leq (1 - M_{m,n,d}^{vehicle})M, \forall (m,n) \in \Psi^{GL},$$

$$\forall d, l = T_{m,d}^{vehicle} + t_{m,d}^{vehicle}$$

Moreover, MBCVs satisfy the following operation constraints

$$T_{0,d}^{vehicle} = 0, \forall d \quad (18)$$

$$\sum_{\forall t} f_{i,t,d}^c \leq 1, \forall i \in \Psi^{GA}, \forall d \quad (19)$$

$$\sum_{\forall t} f_{i,t,d}^c = \sum_{\forall t} l_{i,t,d}^c, \forall i \in \Psi^{GA}, \forall d \quad (20)$$

$$T_{i,d}^{vehicle} \leq \sum_{\forall t} (t \square f_{i,t,d}^c) \leq T_{i,d}^{vehicle} + 1 - \varepsilon, \forall i \in \Psi^{GA}, \forall d \quad (22)$$

$$\sum_{\forall t} (t \square l_{i,t,d}^c) \leq T_{i,d}^{vehicle} + t_{i,d}^{vehicle} + 1 - \varepsilon, \forall i \in \Psi^{GA}, \forall d \quad (23)$$

$$t_{i,d}^{vehicle} \geq 0, \forall i \in \Psi^{GA}, \forall d \quad (24)$$

$$0 \leq T_{i,d}^{vehicle} \leq M \sum_{m \in \Omega^{CA}} M_{m,i,d}^{vehicle}, \forall i \in \Psi^{GA}, \forall d \quad (25)$$

where $f_{i,t,d}^c$ is a binary variable that indicates whether vehicle d arrives at station i at time t . $l_{i,t,d}^c$ is a binary variable that indicates whether vehicle d leaves the station at time t . Constraint (18) ensures that all vehicles start from the depot at time 0. Constraint (19) indicates that a station is visited only once by each MBCV. Constraint (20) suggests that one MBCV should leave the station only if it visits the station. Constraints (21)-(23) are similar to (9) and (10), coupling the binary variables ($f_{i,t,d}^c$, $l_{i,t,d}^c$) with the integer variables ($T_{i,d}^{vehicle}$, $t_{i,d}^{vehicle}$). Constraint (24) indicates that the MBCV stay time is non-negative. In addition, constraint (25) makes sure that vehicle arrive time is equal to 0 if vehicle d did not visit the station.

C. Model of Hydrogen Dynamic Flow

Different from the electricity delivery in power transmission lines, the hydrogen delivery in pipelines follows the aerodynamic laws, and the hydrogen flow will be driven by the pressure along the pipelines in correspondence to the ingredients, temperature, density, etc. The hydrogen states such as velocity, temperature, density, pressure, etc. can be linked by the one-dimensional fluid dynamics along the pipelines. Generally, according to the aerodynamic criteria, the process can be described by the following two equations [36]:

$$\frac{\partial \rho}{\partial t} + \frac{\partial F}{A \partial x} = 0 \quad (26)$$

$$\frac{\partial F}{A \partial t} + \frac{\partial p}{\partial x} + \frac{\lambda}{2d} \frac{F^2}{\rho A^2} = 0 \quad (27)$$

where ρ refers to the hydrogen density; F denotes the hydrogen mass flow rate; p denotes the hydrogen pressure; t denotes to the operation time; x denotes the position in a hydrogen pipeline; A denotes the cross-sectional area of the pipelines; d denotes the diameter of the pipeline; λ denotes the friction coefficient of the pipeline.

This work was performed under the auspices of the U.S. Department of Energy by Lawrence Livermore National Laboratory under Contract DE-AC52-07NA27344 with Release Number LLNL-JRNL-827835.

Since (26) and (27) are partial differential equations and difficult to be solved, they need to be turned into their difference form. Here, the partial differential equations (26) and (27) are approximately transformed in the following *Wendroff* difference form [37], where each partial differential equation is reformulated by $X_{i+1,t+1}$, $X_{i,t+1}$, $X_{i+1,t}$ and, $X_{i,t}$.

$$\frac{\partial X}{\partial t} \approx \frac{1}{2} \left(\frac{X_{i+1,t+1} - X_{i+1,t}}{\Delta t} + \frac{X_{i,t+1} - X_{i,t}}{\Delta t} \right) \quad (28)$$

$$\frac{\partial X}{\partial x} \approx \frac{1}{2} \left(\frac{X_{i+1,t+1} - X_{i+1,t}}{\Delta x} + \frac{X_{i,t+1} - X_{i,t}}{\Delta x} \right) \quad (29)$$

$$X \approx \frac{1}{4} (X_{i+1,t+1} + X_{i,t+1} + X_{i+1,t} + X_{i,t}) \quad (30)$$

where Δt and Δx indicate the time and spatial step, respectively. The second order accuracy with the truncation errors $O(\Delta t^2 + \Delta x^2)$ in (28)-(30) are ignored in this paper.

Thanks to the *Wendroff* difference form, the partial differential equations (26) and (27) can be transformed into (31) and (32), and the transient mass flow in the hydrogen pipelines can be simply expressed by (31)-(32).

$$(\rho_{i+1,t+1} + \rho_{i,t+1} - \rho_{i+1,t} - \rho_{i,t}) + \frac{\Delta t}{\Delta x A} [F_{i+1,t+1} + F_{i+1,t} - F_{i,t+1} - F_{i,t}] = 0 \quad (31)$$

$$\begin{aligned} & \frac{1}{A} [F_{i+1,t+1} + F_{i,t+1} - F_{i+1,t} - F_{i,t}] + \\ & + \frac{\Delta t}{\Delta x} [p_{i+1,t+1} + p_{i+1,t} - p_{i,t+1} - p_{i,t}] \\ & + \frac{\lambda \Delta x}{4dA} \left(\frac{F_{i,t+1}^2}{\rho_{i,t+1}} + \frac{F_{i+1,t+1}^2}{\rho_{i+1,t+1}} + \frac{F_{i+1,t}^2}{\rho_{i+1,t}} + \frac{F_{i,t}^2}{\rho_{i,t}} \right) = 0 \end{aligned} \quad (32)$$

Thus, inspecting the hydrogen flow in pipeline (m, n) gives

$$(\rho_{mn,i+1,t+1} + \rho_{mn,i,t+1} - \rho_{mn,i+1,t} - \rho_{mn,i,t}) + \frac{\Delta t}{\Delta x A_{mn}} [F_{mn,i+1,t+1} + F_{mn,i+1,t} - F_{mn,i,t+1} - F_{mn,i,t}] = 0, \quad (33)$$

$$\forall t = 1, \dots, T-1, \forall i = 0, \dots, \left\lfloor \frac{L_{mn}}{\Delta x} \right\rfloor - 1$$

$$\begin{aligned} & \frac{1}{A_{mn}} [F_{mn,i+1,t+1} + F_{mn,i,t+1} - F_{mn,i+1,t} - F_{mn,i,t}] + \\ & + \frac{\Delta t}{\Delta x} [p_{mn,i+1,t+1} + p_{mn,i+1,t} - p_{mn,i,t+1} - p_{mn,i,t}] \\ & + \frac{\lambda \Delta x}{4dA_{mn}} \left(\frac{F_{mn,i,t+1}^2}{\rho_{mn,i,t+1}} + \frac{F_{mn,i+1,t+1}^2}{\rho_{mn,i+1,t+1}} + \frac{F_{mn,i+1,t}^2}{\rho_{mn,i+1,t}} + \frac{F_{mn,i,t}^2}{\rho_{mn,i,t}} \right) = 0, \end{aligned} \quad (34)$$

$$\forall t = 1, \dots, T-1, \forall i = 0, \dots, \left\lfloor \frac{L_{mn}}{\Delta x} \right\rfloor - 1$$

where L_{mn} denotes the length of pipeline (m, n) .

Note that constraint (34) is a non-linear function and cannot be solved by convex optimization method. So, the relationship

between hydrogen density ρ , hydrogen mass flow rate F , and hydrogen velocity w is applied as [37]-[39].

$$F = A \cdot \rho \cdot w \quad (35)$$

Since the hydrogen velocity wouldn't change too much in the operation state, the second-order term in (34) can be approximately changed into

$$\frac{\lambda \Delta x}{4dA_{mn}} \left(\frac{F_{mn,i,t+1}^2}{\rho_{mn,i,t+1}} + \frac{F_{mn,i+1,t+1}^2}{\rho_{mn,i+1,t+1}} \right. \\ \left. + \frac{F_{mn,i+1,t}^2}{\rho_{mn,i+1,t}} + \frac{F_{mn,i,t}^2}{\rho_{mn,i,t}} \right) \approx \frac{\lambda \Delta x \overline{w_{mn}}}{4d} \left(F_{mn,i,t+1} + F_{mn,i+1,t+1} \right. \\ \left. + F_{mn,i+1,t} + F_{mn,i,t} \right), \quad (36)$$

$$\forall t = 1, \dots, T-1, \forall i = 0, \dots, \left[\frac{L_{mn}}{\Delta x} \right] - 1$$

where $\overline{w_{mn}}$ denotes the average hydrogen velocity in pipeline (m, n) . Thus, constraint (34) can be linearized into (37).

$$\frac{1}{A_{mn}} [F_{mn,i+1,t+1} + F_{mn,i,t+1} - F_{mn,i+1,t} - F_{mn,i,t}] \\ + \frac{\Delta t}{\Delta x} [p_{mn,i+1,t+1} + p_{mn,i+1,t} - p_{mn,i,t+1} - p_{mn,i,t}] \\ + \frac{\lambda \Delta x \overline{w_{mn}}}{4d} \left(F_{mn,i,t+1} + F_{mn,i+1,t+1} \right. \\ \left. + F_{mn,i+1,t} + F_{mn,i,t} \right) = 0, \quad (37)$$

$$\forall t = 1, \dots, T-1, \forall i = 0, \dots, \left[\frac{L_{mn}}{\Delta x} \right] - 1$$

FORMULATION OF THE RESTORATION PROCESS

In this section, a multi-period restoration model for IPHDS considering dynamic hydrogen flow is proposed to maximize the total restored weighted loads. The model aims to determine the optimal routes for RRCs and MBCVs as well as the network reconfiguration with the consideration of the transportation states. The optimization model can be set up as follows.

A. Objective Function

The objective of the MPRM is to quickly pick up critical loads. By properly choosing the weights, we can ensure that high-priority loads are restored first. Mathematically, the objective function is expressed as the sum of weighted loads:

$$obj = \max \left(\sum_t \sum_j z_j^e \frac{P_{j,t}^e}{P_{\max,j}^e} + \sum_t \sum_n z_n^g \frac{F_{n,t}^g}{F_{\max,n}^g} \right) \quad (38)$$

where $P_{j,t}^e$ and $F_{n,t}^g$ denote the restored active power at bus j and restored hydrogen load at node n at time t , respectively; z_j^e and z_n^g denote the power load weight and hydrogen load weight, respectively; $P_{\max,j}^e$ and $F_{\max,n}^g$ denote the upper bound of power load and hydrogen load, respectively.

B. Constraints

The constraints of the model should satisfy the requirement of the secure system operation. Specifically, these constraints will include

1) Power flow constraints

The MPRM for the IPHDS should maintain power flow balance at each time period without the violation of physical limits,

$$\begin{cases} P_{c,t} + P_{h,t} - P_{j,t}^e - P_{q,EHP,t} = \\ \sum_{\forall s \in \delta_t(j)} H_{js,t} - \sum_{\forall i \in \pi_t(j)} H_{ij,t} \\ Q_{c,t} + Q_{h,t} - Q_{j,t} - Q_{q,EHP,t} = \end{cases}, \quad (39)$$

$$\begin{cases} \sum_{\forall s \in \delta_t(j)} G_{js,t} - \sum_{\forall i \in \pi_t(j)} G_{ij,t} \\ \forall c \in D, \forall h \in L, \forall j \in E, \forall q \in \Omega, \forall t = 1, \dots, T \\ Q_{j,t} = \tan \theta_{j,t} P_{j,t}^e, \forall j \in E, \forall t = 1, \dots, T \end{cases} \quad (40)$$

$$\begin{cases} -M \cdot (1 - y_{i,j,t}) \leq V_{j,t} - V_{i,t} - (r_{ij} H_{ij,t} + x_{ij} G_{ij,t}) \\ \leq M \cdot (1 - y_{i,j,t}) \\ H_{ij,t}^2 + G_{ij,t}^2 \leq S_{ij}^{\max} y_{i,j,t} \\ \forall (i, j) \in Y \cup U, \forall t = 1, \dots, T \end{cases}, \quad (41)$$

$$\begin{cases} V_j^{\min} \leq V_{j,t} \leq V_j^{\max}, \\ \forall j \in E, \forall t = 1, \dots, T \end{cases} \quad (42)$$

$$\begin{cases} V_{j,t} = V_j^0, \\ \forall j \in D \cup L, \forall t = 1, \dots, T \end{cases} \quad (43)$$

$$\begin{cases} P_c^{\min} \leq P_{c,t} \leq P_c^{\max} \\ Q_c^{\min} \leq Q_{c,t} \leq Q_c^{\max}, \forall c \in D, \forall t = 1, \dots, T \end{cases} \quad (44)$$

$$\begin{cases} P_h^{\min} \leq P_{h,t} \leq P_h^{\max} \\ Q_h^{\min} \leq Q_{h,t} \leq Q_h^{\max}, \forall h \in L, \forall t = 1, \dots, T \end{cases} \quad (45)$$

$$\begin{cases} P_{q,EHP}^{\min} \leq P_{q,EHP,t} \leq P_{q,EHP}^{\max} \\ Q_{q,EHP}^{\min} \leq Q_{q,EHP,t} \leq Q_{q,EHP}^{\max}, \forall q \in \Omega, \forall t = 1, \dots, T \end{cases} \quad (46)$$

$$(1)-(25) \quad (47)$$

where $P_{c,t}$ and $Q_{c,t}$ are the active and reactive powers of the coal-fired generator connected to bus c at time period t ; $P_{h,t}$ and $Q_{h,t}$ are the active and reactive powers of the hydrogen-fired generator connected to bus h at time period t ; $P_{q,EHP,t}$ is the active power consumption of the EHP connected to bus q at time period t ; $P_{q,EHP}^{\min}$ and $P_{q,EHP}^{\max}$ are the lower and upper bounds of the active power of the EHP connected to bus q ; $Q_{q,EHP}^{\min}$ and $Q_{q,EHP}^{\max}$ are the lower and upper bounds of the reactive power of the EHP connected to bus q ; P_c^{\min} and P_c^{\max} are the lower and upper bounds of the active power of the coal-fired generator connected to bus c ; Q_c^{\min} and Q_c^{\max} are the lower and upper bounds of the reactive power of the coal-fired generator connected to bus c ; P_h^{\min} and P_h^{\max} are the lower and upper bounds of the active power of the hydrogen-fired generator connected to bus h ; Q_h^{\min} and Q_h^{\max} are the lower and upper bounds of the reactive power of the hydrogen-fired generator connected to bus h ; $H_{js,t}$ and $G_{js,t}$ are the active and reactive powers on the power transmission line (j, s) at time period t ; S_{ij}^{\max} is the transmission limit of the power transmission line (i, j) ; $P_{j,t}^e$ and $Q_{j,t}$ are the active and reactive loads of bus j at time period t ; $V_{j,t}$ is the voltage magnitude of bus j at time period t ; $\theta_{j,t}$ is the voltage phase angle of bus j at time period t ; V_j^{\min} and V_j^{\max} are the lower and upper bounds of the voltage magnitude at bus j ; V_j^0 is the specified voltage magnitude at bus j ; M is a large number; $\delta_t(j)$ and $\pi_t(j)$ are

the sets of child buses and parent buses of bus j at time period t ; E denotes the set of electric buses; Δ denotes the set of electric buses connected with coal-fired generators; Λ denotes the set of electric buses connected with the hydrogen-fired generators. Y is the set of the backup reconfigured power lines. Ω is the set of the buses connected with EHPs.

For these constraints in the power system, we assume that the power system and hydrogen system are coupled by hydrogen-fired generators and EHPs. Moreover, (39) denotes the power balance constraint at each bus in the power system. Constraint (40) indicates that the power factor of each bus should be kept within a specified value at each time period. Constraint (41) specifies the voltage drop on each power transmission line, and if the transmission line is out of service, this constraint will not be active. Constraint (42) specifies the upper and lower bounds of the voltage magnitude at each bus, and constraint (43) indicates that the voltage magnitude for the bus connected with coal-fired generators or hydrogen-fired generators will always be specified as the given value. Constraint (44) denotes the power consumption limit of EHPs. Constraints (45) and (46) specify the upper and lower bounds of coal-fired generators and hydrogen-fired generators. (47) denotes the constraints for RCs and MBCVs.

2) Hydrogen flow constraints

In the hydrogen system, the MPRM should maintain hydrogen balance and physical limits, giving

$$K_{i,t} - P_{n,t}^g - K_{b,t} = \sum_{\forall o \in \alpha_t(n)} F_{no,0,t} - \sum_{\forall m \in \beta_t(n)} F_{mn,end,t}, \quad (48)$$

$$\forall n \in Q, \forall i \in Y, \forall b \in \Pi, \forall t = 1, \dots, T$$

$$F_{mn}^{\min} \cdot y_{m,n,t} \leq F_{mn,i,t} \leq F_{mn}^{\max} \cdot y_{m,n,t},$$

$$\forall (m,n) \in P \cup B, \forall t = 1, \dots, T, \quad (49)$$

$$\forall i = 0, \dots, \left\lfloor \frac{L_{mn}}{\Delta x} \right\rfloor$$

$$p_{mn}^{\min} \leq p_{mn,i,t} \leq p_{mn}^{\max}, \forall (m,n) \in P \cup B,$$

$$\forall t = 1, \dots, T, \forall i = 0, 1, \dots, \left\lfloor \frac{L_{mn}}{\Delta x} \right\rfloor \quad (50)$$

$$\rho_{mn}^{\min} \leq \rho_{mn,i,t} \leq \rho_{mn}^{\max}, \forall (m,n) \in P \cup B,$$

$$\forall t = 1, \dots, T, \forall i = 0, \dots, \left\lfloor \frac{L_{mn}}{\Delta x} \right\rfloor \quad (51)$$

$$K_{i,t} = \eta_{i,q} \cdot P_{q,EHP,t}, \quad (52)$$

$$\forall q \in \Omega, \forall i \in Y, \forall t = 1, \dots, T$$

$$K_{b,t} = P_{h,t} / GHV, \quad (53)$$

$$\forall h \in L, \forall b \in \Pi, \forall t = 1, \dots, T \quad (33), (37) \quad (54)$$

where $K_{i,t}$ denotes the hydrogen output of EHP connected to node i at time period t ; $K_{b,t}$ denotes the consumption of hydrogen-fired generator connected to node b at time period t ; F_{mn}^{\min} and F_{mn}^{\max} are the lower and upper bounds of the hydrogen mass flow rate in pipeline (m,n) ; p_{mn}^{\min} and p_{mn}^{\max} are the lower and upper bounds of the hydrogen pressure in pipeline (m,n) ; ρ_n^{\min} and ρ_n^{\max} denote the lower and upper bounds of the hydrogen density

in pipeline (m,n) ; $\eta_{i,q}$ is the conversion factor of EHP allocated at hydrogen node i and electric bus q , and GHV is the hydrogen gross heating value; $\alpha_t(n)$ and $\beta_t(n)$ are the sets of child and parent nodes of node n at time period t ; Θ is the set of hydrogen nodes; Π is the set of hydrogen pipelines; B is the set of backup reconfigured pipelines. γ is the set of hydrogen nodes connected to the EHPs. Π is the set of hydrogen nodes connected to the hydrogen-fired generators.

For these constraints in the hydrogen system, we assume that the hydrogen loads are only supplied by EHPs, and the hydrogen flow will be dynamically changing in pipelines. Moreover, constraint (48) denotes the hydrogen flow balance at each node. Constraint (49) denotes the limit of the hydrogen mass flow rate. Constraint (50) denotes the limit of the hydrogen pressure for each pipeline. Constraint (51) denotes the limit of hydrogen density for each pipeline. Constraints (52) and (53) refer to the conversion relationship between EHPs and hydrogen-fired generators. Constraint (54) gives the dynamic hydrogen flow for each pipeline.

3) Network reconfiguration constraints

To improve the resilience of IPHDS, the network reconfiguration strategy has been adopted in the MPRM, yielding the following constraints:

$$y_{i,j,t} = u_{i,j,t}, \forall (i,j) \in U, \forall t = 1, \dots, T \quad (55)$$

$$\sum_{\forall (i,j) \in U} u_{i,j,t} \leq u_t^{\max}, \forall t = 1, \dots, T \quad (56)$$

$$\sum_{\forall t} u_{i,j,t} \leq 1, \forall (i,j) \in U \quad (57)$$

$$y_{m,n,t} = r_{m,n,t}, \forall (m,n) \in B, \forall t = 1, \dots, T \quad (58)$$

$$\sum_{\forall (m,n) \in B} r_{m,n,t} \leq r_t^{\max}, \forall t = 1, \dots, T \quad (59)$$

$$\sum_{\forall t} r_{m,n,t} \leq 1, \forall (m,n) \in B \quad (60)$$

where $u_{i,j,t}$ is a binary variable indicating whether power line (i,j) is reconfigured at time period t : if it is reconfigured, $u_{i,j,t} = 1$; 0 otherwise. $r_{m,n,t}$ is a binary variable which indicates whether pipeline (m,n) is reconfigured at time period t ; u_t^{\max} denotes the maximum number of the reconfigured lines at time period t ; r_t^{\max} denotes the maximum number of the reconfigured pipelines at time period t . Functions (55) and (58) are the reconfiguration state constraints, denoting that if a power line or pipeline is reconfigured, it would follow the power flow constraints and the hydrogen flow constraints. Constraints (56) and (59) shows the limits of reconfigured power lines and pipelines at each time period. Constraints (57) and (60) indicate that each power line or pipeline should only be reconfigured once during an outage.

Therefore, the MPRM for IPHDS can be finally set up with the objective function (38), subject to power system constraints (39)-(47); hydrogen system constraints (48)-(54); and network reconfiguration constraints (55)-(60).

III. CASE STUDIES

In this section, an IPHDS integrated by a modified IEEE 33-bus distribution system and a 48-node hydrogen system is employed to show the effectiveness of the proposed model, the topology of which is depicted in Fig.2. Power buses 1, 15 and 29 are connected with coal-fired generators, while power buses 6,

9, 17, 21 and 23 are connected with both hydrogen-fired generators and hydrogen nodes 9, 7, 20, 24, 37. Besides, we prioritize all power loads into five levels, demonstrating the load priority in [40]. The power loads with the highest priority are located at buses 4, 19, 25, while the power loads with the second-highest priority are located at buses 9, 26, 27.

In the 48-node hydrogen system, nodes 2, 11, 16, 23 and 39 are source nodes connected with EHPs. These nodes are also connected to power buses 3, 16, 19, 25 and 30, respectively. Other nodes are all connected with hydrogen loads. Similarly, hydrogen loads are also prioritized into five levels, with hydrogen loads at nodes 4 and 15 being prioritized the highest level, and loads at nodes 1 and 18 being prioritized the second-highest level. Note that nodes 7, 9, 20, 24 and 37 are connected with the power distribution system via hydrogen-fired generators. To guarantee the hydrogen supply, the loads at nodes 7 and 20 also have the highest priority.

To quantify the restoration performance, the load restoration time is defined as the total required time to recover the load. Besides, we assume that there are two repair crews and two MBCVs in the power system while two repair crews in the hydrogen system. Moreover, the travel time for each RC and MBCV among faulted lines is detailed in [40].

TABLE I REPAIR TIME OF RRCs IN THE 33-BUS SYSTEM

Outages	Repair time (minutes)	
	Repair Crew 1	Repair Crew 2
Fault 1	120	60
Fault 2	120	60
Fault 3	60	120
Fault 4	60	60

TABLE II REPAIR TIME OF RRCs IN THE 48-NODE SYSTEM	Repair time (minutes)	
	Repair Crew 3	Repair Crew 4
Fault 5	120	60
Fault 6	60	60
Fault 7	180	120
Fault 8	120	120
Fault 9	120	60
Fault 10	60	60
Fault 11	120	120
Fault 12	120	60

The RC and MBCV routes are also depicted in Fig. 2, where the islands will be reconnected and the loads will be restored once the faulted lines are repaired. In the 33-bus power system, since Fault 1 and Fault 3 are closer to the RC depot, these two power lines are firstly repaired. Before Fault 1 and Fault 3 are repaired, critical loads at buses 4 and 19 would be islanded. At this time, two MBCVs leave the MBCV depot to buses 4 and 19, and MBCVs will return to the depot sequentially after Fault 3 and Fault 2 are repaired. Then, when RC1 completes the repair task at Fault 1, RC2 has already finished the repair task at Fault 3. Since Fault 2 is closer to Fault 3 and the travel time between Fault 3 to Fault 4 is much longer than that between Fault 2 to Fault 3, RC2 then repairs Fault 2 firstly. Meanwhile, RC1 comes to Fault 5 to finish the repair task although the travel time between Fault 1 and Fault 5 is much longer than other routes. Finally, when Fault 4 and Fault 5 are repaired, the RCs would return to the depot sequentially.

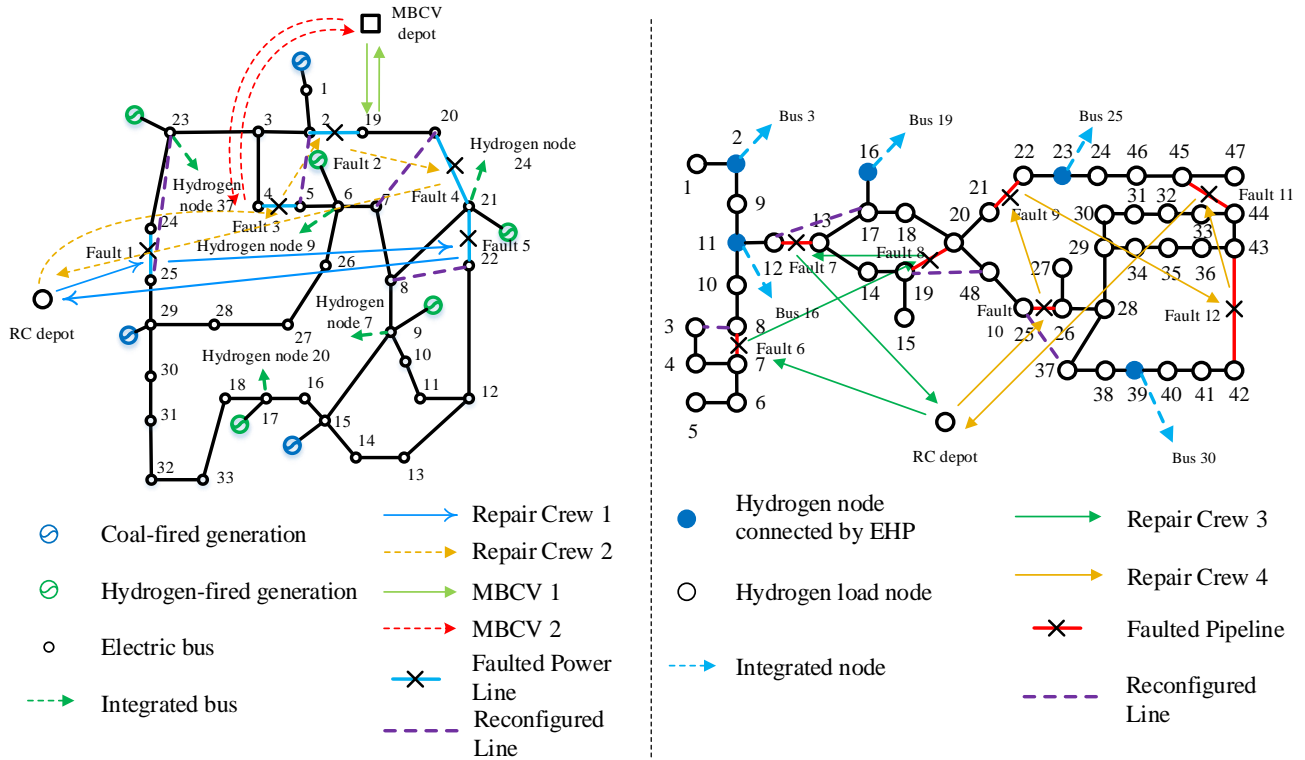


Fig. 2 RC and MBCV routes in the 33-bus-48-node IPHDS

In addition, the hydrogen flow in pipelines are shown in Fig. 3. For each pipeline, the hydrogen flow dynamically changes. This work was performed under the auspices of the U.S. Department of Energy by Lawrence Livermore National Laboratory under Contract DE-AC52-07NA27344 with Release Number LLNL-JRNL-827835.

when the outages happen. Different from the power flow in the power system, when the network topology changes, the

hydrogen flow cannot change immediately. Take pipeline 2-9 as an example. When pipeline 7-8 is damaged, though the hydrogen loads at nodes 3, 4, 5, 6, and 7 are shed, the hydrogen flow in the pipeline cannot decrease immediately to meet the load demand. The excess hydrogen will become to line pack restoration in pipelines. Then, the hydrogen flow in pipeline 2-9 will keep decreasing to a steady-state and meet the load demand in the next 120 minutes. After pipeline 7-8 having been repaired, the hydrogen flow in pipeline 2-9 has to increase to support hydrogen loads at nodes 3, 4, 5, 6, and 7, and will reach a steady-state after the 400-th minute. Besides, Fig. 3 also shows the hydrogen flow in pipeline 7-8, which has been damaged in the disaster. In the first 110 minutes, the hydrogen flow will remain 0 since pipeline 7-8 has not been repaired. After the 110-th minute, the hydrogen flow will dynamically increase and will reach the steady-state at the 360-th minutes.

To investigate the influence of RCs, MBCVs, the dynamic hydrogen flow, and transportation states in the IPHDS restoration, we compare the restoration time and restored weighted loads in five cases:

- Case 1: no RCs and MBCVs;
- Case 2: 4 RCs and 2 MBCVs;
- Case 3: 4 RCs and 2 MBCVs with the consideration of the dynamic hydrogen flow model;
- Case 4: 4 RCs and 2 MBCVs with the consideration of the transportation state;
- Case 5: 4 RCs and 2MBCVs with the consideration of the dynamic hydrogen flow and the transportation state.

In Fig. 4, compared with the results of Case 1 and Case 2, it is observed that with the help of RCs and MBCVs, the IPHDS will restore faster in Case 2. And when the dynamic hydrogen flow model is applied to the IPHDS, since the hydrogen flow cannot change instantaneously with the load demand, the weight load restoration will slightly lag behind the network repairing and reconfiguration, which can be observed from the results of Case 2 and Case 3. On the other hand, if the transportation states are considered in the restoration process, due to the traffic congestion and travel time, the repair order of faulted lines in Case 4 will be different from that in Case 2. For that reason, the weighted load in Case 2 will restore faster than that in Case 4 before the 200-th minute. But after the 200-th minute, the load in Case 4 will restore a little faster than that in Case 2, thanks for the rational optimization of the RC routes. Finally, combined with the dynamic hydrogen flow model and transportation states, the weighted load restoration process is shown in Case 5.

In the hydrogen system, RCs will first repair Fault 6 and Fault 10 since they are close to the depot. Once Fault 6 and Fault 10 are recovered, two islands in the hydrogen system will be reconnected and the corresponding hydrogen loads are picked up. Next, Fault 8 and Fault 9 are repaired. Though Fault 8 is farther than Fault 7 from Fault 6, the travel time between Fault 8 and Fault 6 is shorter than that between Fault 7 and Fault 6 due to the traffic congestion. For the same reason, at the next time period, Fault 7 and Fault 12, rather than Fault 11, will be repaired. Fault 11 will be repaired by RC4 after finishing the repair task at Fault 12. Finally, RC3 and RC4 will return to the depot after all repair tasks are finished.

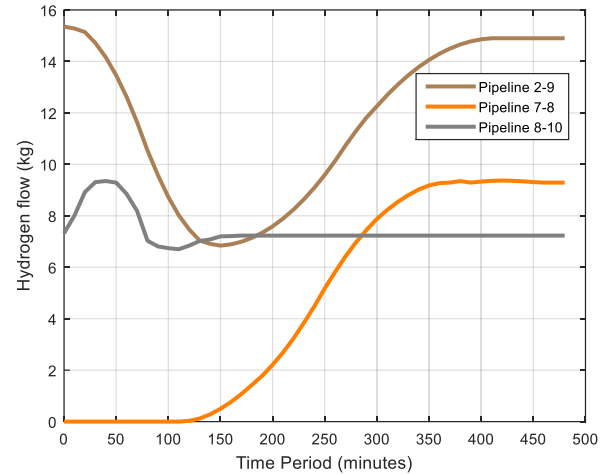


Fig.3 Hydrogen flow in classic pipelines

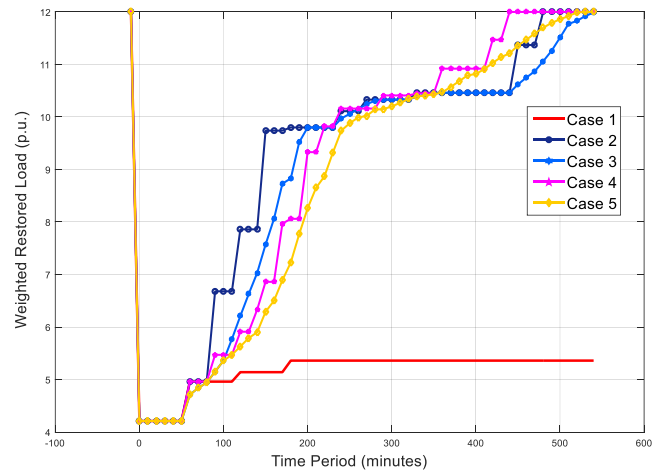


Fig. 4 Restored weighted loads in the 33-bus-48-node IPHDS

IV. CONCLUSION

This paper proposes a multiperiod restoration model for an integrated power and hydrogen distribution system with RCs, MBCVs, dynamic hydrogen flow, and transportation states. Once the outage happens, the network reconfiguration will be first applied to avoid islanding. Then, RCs will be quickly dispatched to repair faulted lines under the consideration of the transportation state. MBCVs will also be dispatched to cooperate with RCs and support critical loads which are located in islands. Numerical results show that the hydrogen flow and hydrogen load restoration will be slightly lag behind the pipeline repair and reconfiguration. Moreover, transportation states will influence the RC repair orders and routes. Therefore, considering dynamic hydrogen flow model and the transportation states, the restoration strategy will be much more realistic and viable, although the restoration time will be a little longer.

REFERENCES

- [1] Z. Bie, Y. Lin, G. Li, and F. Li, "Battling the Extreme: A Study on the Power System Resilience," *Proc. IEEE*, vol. 105, no. 7, pp. 1253-1266, 2017.
- [2] T. Ding, M. Qu, Z. Wang, B. Chen, C. Chen, and M. Shahidehpour, "Power System Resilience Enhancement in Typhoons Using A Three-Stage Day-Ahead Unit Commitment," *IEEE Trans. Smart Grid*, Early Access, 2020.

- [3] Y. Wang, C. Chen, J. Wang, and R. Baldick, "Research on Resilience of Power Systems Under Natural Disasters—A Review," *IEEE Trans. Power Syst.*, vol. 31, no. 2, pp. 1604-1613, 2016.
- [4] P. Hoffman and W. Bryan, "Comparing the Impacts of Northeast Hurricanes on Energy Infrastructure," U.S. Department of Energy, Washington DC, USA 2013.
- [5] Executive Office of the President, Economic Benefits of Increasing Electric Grid Resilience to Weather Outages, Tech. Rep., 2013.
- [6] Z. Li, M. Shahidehpour, F. Aminifar, A. Alabdulwahab, and Y. Al-Turki, "Networked Microgrids for Enhancing the Power System Resilience," *Proc. IEEE*, vol. 105, no. 7, pp. 1289-1310, 2017.
- [7] W. Yuan, J. Wang, F. Qiu, C. Chen, C. Kang, and B. Zeng, "Robust Optimization-Based Resilient Distribution Network Planning Against Natural Disasters," *IEEE Trans. Smart Grid*, vol. 7, no. 6, pp. 2817-2826, 2016.
- [8] X. Wang, Z. Li, M. Shahidehpour, and C. Jiang, "Robust Line Hardening Strategies for Improving the Resilience of Distribution Systems With Variable Renewable Resources," *IEEE Trans. Sustain. Energy*, vol. 10, no. 1, pp. 386-395, 2019.
- [9] N. L. deghani, A. B. Jeedi and A. Shafieezadeh, "Intelligent hurricane resilience enhancement of power distribution systems via deep reinforcement learning," *Appl. Energy*, vol. 285, p. 116355, 2021.
- [10] B. Chen, C. Chen, J. Wang, K. L. Butler-Purpy, and A. I. U. S. Argonne National Lab. ANL, "Sequential Service Restoration for Unbalanced Distribution Systems and Microgrids," *IEEE Trans. Power Syst.*, vol. 33, no. 2, pp. 1507-1520, 2018.
- [11] F. Shen, Q. Wu, J. Zhao, W. Wei, N. D. Hatziargyriou, and F. Liu, "Distributed Risk-Limiting Load Restoration in Unbalanced Distribution Systems With Networked Microgrids," *IEEE Trans. Smart Grid*, vol. 11, no. 6, pp. 4574-4586, 2020.
- [12] T. Ding, Y. Lin, Z. Bie, and C. Chen, "A resilient microgrid formation strategy for load restoration considering master-slave distributed generators and topology reconfiguration," *Appl. Energy*, vol. 199, pp. 205-216, 2017.
- [13] Y. Lin and Z. Bie, "Tri-level optimal hardening plan for a resilient distribution system considering reconfiguration and DG islanding," *Appl. Energy*, vol. 210, pp. 1266-1279, 2018.
- [14] J. Liu, Y. Yu and C. Qin, "Unified two-stage reconfiguration method for resilience enhancement of distribution systems," *IET Gener. Transm. Distrib.*, vol. 13, no. 9, pp. 1734-1745, 2019.
- [15] J. Xu, T. Zhang, Y. Du, W. Zhang, T. Yang, and J. Qiu, "Islanding and dynamic reconfiguration for resilience enhancement of active distribution systems," *Electr. Pow. Syst. Res.*, vol. 189, p. 106749, 2020.
- [16] S. Lei, C. Chen, Y. Song, and Y. Hou, "Radiality Constraints for Resilient Reconfiguration of Distribution Systems: Formulation and Application to Microgrid Formation," *IEEE Trans. Smart Grid*, vol. 11, no. 5, pp. 3944-3956, 2020.
- [17] Q. Shi, F. Li, M. Olama, J. Dong, Y. Xue, M. Starke, C. Winstead, and T. Kuruganti, "Network reconfiguration and distributed energy resource scheduling for improved distribution system resilience," *Int. J. Electr. Power Energy Syst.*, vol. 124, p. 106355, 2021.
- [18] G. Glenk and S. Reichelstein, "Economics of converting renewable power to hydrogen," *Nat. Energy*, vol. 4, no. 3, pp. 216-222, 2019.
- [19] G. Pan, W. Gu, Y. Lu, H. Qiu, S. Lu, and S. Yao, "Optimal Planning for Electricity-Hydrogen Integrated Energy System Considering Power to Hydrogen and Heat and Seasonal Storage," *IEEE Trans. Sustain. Energy*, vol. 11, no. 4, pp. 2662-2676, 2020.
- [20] M. Shahidehpour, X. Wang, C. Shao, X. Wang, Q. Zhou, and C. J. Feng, "Optimal Stochastic Operation of Integrated Electric Power and Renewable Energy with Vehicle-Based Hydrogen Energy System," *IEEE Trans. Power Syst.*, Early Access, 2021.
- [21] Y. Tao, J. Qiu, S. Lai, and J. Zhao, "Integrated Electricity and Hydrogen Energy Sharing in Coupled Energy Systems," *IEEE Trans. Smart Grid*, Early Access, 2020.
- [22] J. Li, J. Lin, Y. Song, X. Xing, and C. Fu, "Operation Optimization of Power to Hydrogen and Heat (P2HH) in ADN Coordinated With the District Heating Network," *IEEE Trans. on Sustain. Energy*, vol. 10, no. 4, pp. 1672-1683, 2019.
- [23] M. Ban, J. Yu, M. Shahidehpour, and Y. Yao, "Integration of power-to-hydrogen in day-ahead security-constrained unit commitment with high wind penetration," *J. Mod. Power Syst. Clean Energy*, vol. 5, no. 3, pp. 337-349, 2017.
- [24] T. Yun, W. Zedi, L. Yan, M. Qian, H. Qian, L. Shubin, G. L. E. P. State, D. A. C. C. Power, U. O. T. Shenyang, and G. E. I. M. State, "Multi energy storage system model based on electricity heat and hydrogen coordinated optimization for power grid flexibility," *CSEE J. Power Energy Syst.*, vol. 5, no. 2, pp. 266-274, 2019.
- [25] S. Lei, C. Chen, Y. Li, and Y. Hou, "Resilient Disaster Recovery Logistics of Distribution Systems: Co-Optimize Service Restoration With Repair Crew and Mobile Power Source Dispatch," *IEEE Trans. Smart Grid*, vol. 10, no. 6, pp. 6187-6202, 2019.
- [26] B. Chen, Z. Ye, C. Chen, J. Wang, T. Ding, Z. Bie, and A. I. U. S. Argonne National Lab. ANL, "Toward a Synthetic Model for Distribution System Restoration and Crew Dispatch," *IEEE Trans. Power Syst.*, vol. 34, no. 3, pp. 2228-2239, 2019.
- [27] S. Lei, J. Wang, C. Chen, Y. Hou, and A. I. U. S. Argonne National Lab. ANL, "Mobile Emergency Generator Pre-Positioning and Real-Time Allocation for Resilient Response to Natural Disasters," *IEEE Trans. Smart Grid*, vol. 9, no. 3, pp. 2030-2041, 2018.
- [28] T. Paolo and V. Daniele, *The vehicle routing problem*: Society for Industrial and Applied Mathematics, 2002.
- [29] Y. Lin, B. Chen, J. Wang, and Z. Bie, "A Combined Repair Crew Dispatch Problem for Resilient Electric and Natural Gas System Considering Reconfiguration and DG Islanding," *IEEE Trans. Power Syst.*, vol. 34, no. 4, pp. 2755-2767, 2019.
- [30] Y. Xu, Y. Wang, J. He, M. Su, and P. Ni, "Resilience-Oriented Distribution System Restoration Considering Mobile Emergency Resource Dispatch in Transportation System," *IEEE Access*, vol. 7, pp. 73899-73912, 2019.
- [31] A. Arif, Z. Wang, J. Wang, and C. Chen, "Power Distribution System Outage Management With Co-Optimization of Repairs, Reconfiguration, and DG Dispatch," *IEEE Trans. Smart Grid*, vol. 9, no. 5, pp. 4109-4118, 2018.
- [32] G. Zhang, F. Zhang, X. Zhang, Z. Wang, K. Meng, and Z. Y. Dong, "Mobile Emergency Generator Planning in Resilient Distribution Systems: A Three-Stage Stochastic Model With Nonanticipativity Constraints," *IEEE Trans. Smart Grid*, vol. 11, no. 6, pp. 4847-4859, 2020.
- [33] T. Ding, Z. Wang, W. Jia, B. Chen, C. Chen, and M. Shahidehpour, "Multiperiod Distribution System Restoration With Routing Repair Crews, Mobile Electric Vehicles, and Soft-Open-Point Networked Microgrids," *IEEE Trans. Smart Grid*, vol. 11, no. 6, pp. 4795-4808, 2020.
- [34] R. Teixeira Pinto, M. Aragues-Penalba, O. Gomis-Bellmunt, and A. Sumper, "Optimal Operation of DC Networks to Support Power System Outage Management," *IEEE Trans. Smart Grid*, vol. 7, no. 6, pp. 2953-2961, 2016.
- [35] T. Ding, R. Bo, W. Gu, and H. Sun, "Big-M Based MIQP Method for Economic Dispatch with Disjoint Prohibited Zones," *IEEE Trans. Power Syst.*, vol. 29, no. 2, pp. 976-977, 2014.
- [36] J. Fang, Q. Zeng, X. Ai, Z. Chen, and J. Wen, "Dynamic Optimal Energy Flow in the Integrated Natural Gas and Electrical Power Systems," *IEEE Trans. on Sustain. Energy*, vol. 9, no. 1, pp. 188-198, 2018.
- [37] A. R. Gourlay and J. L. Morris, "Finite-Difference Methods for Nonlinear Hyperbolic Systems," *Math. Comput.*, vol. 22, no. 101, pp. 28-39, 1968.
- [38] M. Behbahani-Nejad and Y. Shekari, "Reduced order modeling of natural gas transient flow in pipelines," *Int. J. Eng. Appl. Sci.*, vol. 7, no. 5, pp. 148-152, 2008.
- [39] A. D. Woldeyohannes and M. A. A. Majid, "Simulation model for natural gas transmission pipeline network system," *Simul. Model. Pract. Theory*, vol. 19, no. 1, pp. 196-212, 2011.
- [40] <https://github.com/ZekaiWang-XJTU/data-of-33-bus-distribution-network>